

1 **The rain is askew: Two idealized models relating the vertical velocity and**
2 **precipitation distributions**

3 Angeline G. Pendergrass*

4 *National Center for Atmospheric Research, Boulder, Colorado, USA.*

5 Edwin P. Gerber

6 *Center for Atmosphere and Ocean Sciences, Courant Institute, New York University, New York,*
7 *New York*

8 *Corresponding author address: Angeline G. Pendergrass, P.O. Box 3000, Boulder, CO 80307.

9 The National Center for Atmospheric Research is sponsored by the National Science Foundation.

10 E-mail: apgrass@uw.edu

ABSTRACT

11 As the planet warms, climate models predict that rain will become heavier
12 but less frequent, and that the circulation will weaken. Here, two heuristic
13 models relating moisture, vertical velocity, and rainfall distributions are de-
14 veloped, one in which the distribution of vertical velocity is prescribed and
15 another in which it is predicted. These models are used to explore the re-
16 sponse to warming and moistening, changes in the circulation, atmospheric
17 energy budget, and stability. Some key assumptions of the models include that
18 relative humidity is fixed within and between climate states and that stability
19 is constant within each climate state. The first model shows that an increase
20 in skewness of the vertical velocity distribution is crucial for capturing salient
21 characteristics of the changing distribution of rain, including the muted rate of
22 mean precipitation increase relative to extremes and the decrease in the total
23 number or area of rain events. The second model suggests that this increase
24 in the skewness of the vertical velocity arises from the asymmetric impact of
25 latent heating on vertical motion.

1. Introduction

Changes in rain are inexorably tied to changes in atmospheric circulation. In response to global warming, climate model projections show an increase in global-mean precipitation, the rate of which is in balance with the change in atmospheric radiative cooling (O’Gorman et al. 2012; Pendergrass and Hartmann 2014a). This rate of increase, 1-3% per degree of warming across climate models, is smaller than the rate of increase of moisture in the atmosphere, which roughly follows saturation vapor pressure at $\sim 7\% \text{ K}^{-1}$ (Held and Soden 2006). The difference between the rates of increase of moisture and precipitation with warming imply a slowing of the atmospheric overturning circulation (Betts 1998). The weakening circulation in climate model projections manifests as a decrease in spatial variance of convective mass flux (Held and Soden 2006) and the Walker circulation (the anti-symmetric component of variance of 500 hPa vertical velocity in the tropics, Vecchi and Soden 2007).

Along with changes in circulation, climate model projections show changes in the distribution of rainfall, as shown in Fig. 1 from version 5 of the Coupled Model Intercomparison Project (for CMIP5, Taylor et al. 2012, following Pendergrass and Hartmann 2014b). More rain falls at heavier rain rates, less rain falls at moderate rain rates, and the number of rainy days decreases. These changes in the distribution of rainfall in response to warming (both induced by increasing carbon dioxide forcing and between El Niño and La Nina phases of ENSO) in models can be well described by two empirically derived patterns, denoted the “shift” and “increase” modes (Pendergrass and Hartmann 2014c), which are illustrated in Fig. 2.

The “increase” mode (Fig. 2a,b) characterizes an increase in the frequency of rain by the same fraction at all rain rates. The bell shape of the distribution, when plotted as a function of $\log(\text{rain rate})$ in Fig. 2a, simply follows the climatological distribution of rain frequency. While the change

49 in rain amount is characterized by a similar bell-shaped pattern, it occurs at higher rain rates
50 (Fig. 2b). The total amount of rain is the product of the rain frequency and rain rate, such that an
51 increase in rain frequency at higher rain rates has a larger impact on the total precipitation than it
52 does at lower rain rates. An increase in rain frequency implies a reduction in the number of dry
53 days. In the global mean, it rains about half of the time, such that a one percent increase at all rain
54 rates is associated with a one-half percent reduction in dry days.

55 The “shift” mode (Fig. 2c,d) characterizes a movement of the distribution of rain to higher rain
56 rates, but with no net increase in the total rain amount. It is defined as a shift of the rain amount
57 distribution (Fig. 2d); the corresponding change in the rain frequency distribution can also be
58 obtained (Fig. 2c). A larger decrease in the frequency of light rain events is needed to offset the
59 smaller increase in the frequency of strong rain events on total precipitation, hence the shift mode
60 is associated with an increase in the number of dry days. For a one percent increase in the shift
61 mode, the total number of dry days increases by about one-half of a percent.

62 Pendergrass and Hartmann (2014b) found that a combination of the shift and increase modes
63 could capture most of the change in the distribution of rain in most climate model simulations of
64 global warming, and the entire change in some models. The essence of their result can be found by
65 comparing Fig. 1c and d with Fig. 2e and f: the combination of shift and increase modes optimally
66 fitted to the multi-model mean change in the rain distribution. The response of the shift mode is
67 larger than the increase mode, such that there is a modest increase in the frequency of dry days.

68 Not all of the change in the distribution of rain in climate models is captured by the shift and
69 increase modes. Pendergrass and Hartmann (2014c) identified two additional aspects of the chang-
70 ing distribution of rain common to many models: the light rain mode and the extreme mode. The
71 light rain mode is the small increase in rain frequency just below 1 mm d^{-1} visible in Fig. 1c, also
72 evident in Lau et al. (2013). The extreme mode represents additional increases in rain at the heav-

73 uest rain rates, beyond what is captured by the shift and increase modes. It is crucial for capturing
74 the response of extreme precipitation to warming.

75 Changes in moisture, circulation, and the distribution of rain in response to warming are related.
76 Indeed, the changes in the intensity of extreme rain events in climate model projections of global
77 warming can be linearly related to changes in moisture and vertical velocity in most models and
78 regions (Emori and Brown 2005; O’Gorman and Schneider 2009; Chou et al. 2012). This moti-
79 vates us to consider whether we can understand the changing distribution of rain in terms of the
80 changes in moisture and vertical velocity distributions, constituting a physically based, rather than
81 empirically derived, approach.

82 One might assume that changes in the distribution of rain are complex. The distribution of rain
83 (particularly the global distribution) is generated by a number of different types of precipitating
84 systems, each of which is driven by somewhat different mechanisms and might respond differently
85 to external forcing. For example, it would not be surprising if midlatitude cyclones and tropical
86 convection responded differently to global warming. On the other hand, we expect many aspects of
87 the response to warming to be fairly straightforward: warming along with moistening at a relative
88 humidity that stays constant on surfaces of constant temperature (Romps 2014).

89 In this study, we approach the relationships among changes in moisture, vertical velocity, and
90 rain by examining the response to straightforward changes of simple statistical distributions. We
91 develop two heuristic models that predict the distribution of rain from moisture and vertical veloc-
92 ity distributions. We will see that despite the potential for complexity among these relationships,
93 we can recover many aspects of the changes in rainfall and vertical velocity we see in climate
94 models in an idealized setting.

95 In Section 2, we introduce the first model, in which distributions of moisture and vertical velocity
96 are prescribed. We use the model to explore how the distribution of rain responds to warming and

97 moistening, and to changes in the strength and asymmetry (or skewness) of the vertical velocity
98 distribution. Then, in Section 3, we introduce a second model that predicts the vertical velocity
99 distribution in order to understand its changes in concert with those of the distribution of rain.
100 In Section 4, we show that climate model simulations also have increasing skewness of vertical
101 velocity with warming. Finally, we consider the implications of the increasing skewness of vertical
102 velocity on convective area in Section 5 and conclude our study in Section 6.

103 **2. The first model: Prescribed vertical velocity**

104 We know rain is a result of very complex processes, many of which are parameterized rather than
105 explicitly modeled in climate models. At the most basic level, rain is regulated by two processes:
106 (1) the moisture content, which is tied to the temperature structure, assuming constant relative
107 humidity, and (2) the magnitude of upward vertical velocity. Instead of considering variability
108 in space, consider a distribution that captures the structure of all regions globally. Furthermore,
109 neglect concerns about the vertical structure of the motion or the structure of the atmosphere, and
110 consider only the vertical flux of moisture through the cloud base.

111 The key – and gross – simplification of this model is that we will assume that the vertical velocity
112 is *independent* of the temperature and moisture content, so we can model these as two independent
113 distributions. We know this is not the case – upward velocity is often driven by convection, which
114 occurs where surface temperature is warm – but for now we will see what insight can be gleaned
115 with this assumption.

116 *a. Model description*

117 Our first model is driven by two prescribed, independent, Gaussian (normal) distributions: one
118 for temperature, $N(\bar{T}, \sigma_T)$, where \bar{T} is the mean temperature and σ_T is width of the temperature

119 distribution, and another for vertical velocity, $N(\bar{w}, \sigma_w)$, where \bar{w} is the mean vertical velocity
 120 (equal to zero when mass is conserved) and σ_w is the width of the w distribution. The tempera-
 121 ture distribution, with the assumption of constant relative humidity, in turn gives us the moisture
 122 distribution. We calculate moisture q ,

$$q(T) = q_0 e^{0.07T}, \quad (1)$$

123 where q_0 is chosen so that $q(T)$ is equal to its Clausius-Clapeyron value at $T = 287$ K. This
 124 equation is very similar to Clausius-Clapeyron, except that here $dq/dT = 7 \%$ K^{-1} exactly. The
 125 implied relative humidity is fixed at 100%. The choice of 100% relative humidity is arbitrary, but
 126 any non-zero choice that is held constant will result in the same behavior.

127 We suppose that it rains whenever vertical velocity w is positive (upward), with a rain rate equal
 128 to the product of the moisture, vertical velocity, and air density ρ_a (held constant at 1.225 kg m^{-3} ,
 129 its value at sea level and 15°C),

$$r(q, w) = \begin{cases} \rho_a w q, & w > 0 \\ 0, & w \leq 0. \end{cases} \quad (2)$$

130 This is analogous to saying that the rain rate is equal to the flux of moisture across the cloud base.
 131 While this is a gross simplification, it would hold if the column were saturated and the temperature
 132 structure fixed, and the air was lifted to a level where there the saturation specific humidity is
 133 effectively zero. In this limit, any moisture advected upward will lead to supersaturation and
 134 rain from above. Neglecting the impact of condensation on the temperature is a similarly coarse
 135 approximation as our assumption that the temperature and vertical velocity are independent.

136 The rain frequency distribution is obtained by integrating across the distributions of T (which
 137 determines q by Eqn. 1) and w ,

$$p(r) = \int_0^{\infty} \int_{-\infty}^{\infty} \int_{-\infty}^{\infty} \delta(r - \rho_a w q) \rho_a w q p(T) p(w) dT dw dr, \quad (3)$$

138 where $p(T)$ and $p(w)$ are Gaussian probability density functions and δ is a Dirac delta function.

139 The rain amount distribution is then,

$$P(r) = r p(r). \quad (4)$$

140 Lastly, we must specify the parameters governing the temperature and vertical velocity distribu-
 141 tions, which are listed in Table 1 for reference. For temperature (shown in Fig. 3a) we take \bar{T} to
 142 be 287 K and its standard deviation $\sigma_T = 16$ K, both chosen to match the surface air temperature
 143 distribution in a climate model. The vertical velocity distribution (shown in Fig. 3b) must have
 144 a mean $\bar{w} = 0$ if mass is to be conserved. Given the temperature distribution above, the standard
 145 deviation of w will ultimately set the total precipitation. Thus we sought to constrain its value
 146 so as to capture the total precipitation in climate models and observational datasets like GPCP
 147 One-Degree Daily (see Pendergrass and Hartmann 2014c), while at the same time being consis-
 148 tent with the vertical velocity distribution in climate models. Studies such as Emori and Brown
 149 (2005) show that rain frequency changes are linearly related to changes in moisture and 500 hPa
 150 vertical velocity in many climate models for most regions. While vertical velocity at cloud base
 151 rather than 500 hPa would be more closely physically related to our conceptual model, it is not
 152 archived for these climate model integrations.

153 The rain frequency distribution (shown in Fig. 3c) is calculated numerically following the de-
 154 scription in Appendix A. It is dry exactly 50% of the time, since the vertical velocity distribution
 155 is symmetric about zero. The peak of the rain frequency distribution occurs at just under 10 mm
 156 d^{-1} . The rain amount distribution (Fig. 3d) shows how much rain falls in each rain rate bin. The

157 peak of the rain amount distribution occurs at a rain rate about an order of magnitude larger than
158 for the rain frequency distribution.

159 These distributions resemble distributions in observational datasets and climate models to the
160 correct order of magnitude – compare to Fig. 1a,b and Pendergrass and Hartmann (2014c) – despite
161 the crude assumptions of our model. The main deficiency of our model compared to climate
162 models is a lack of precipitation at light rain rates, and a corresponding overestimation of dry-day
163 frequency. However, climate models underestimate the dry-day frequency by about a factor of two
164 compared to GPCP 1DD and TRMM 3B42 observational datasets (Pendergrass and Hartmann
165 2014c). The implications of this discrepancy on the rain amount distribution are nonetheless small
166 because light rain contributes less than heavy rain does to the total precipitation, so that distribution
167 of rain amount appears better than rain frequency qualitatively (compare Figs. 1b and 3d).

168 The goal in developing this toy model is to explore what happens in response to perturbations:
169 warming and moistening, weakening of the circulation, and introducing skewness to the vertical
170 velocity distribution.

171 *b. Response to warming and moistening*

172 We approximate warming by simply shifting the mean of the temperature distribution \bar{T} 1 degree
173 K higher. We keep σ_T constant, assuming no change in the variance of temperature. The moisture
174 distribution adjusts accordingly. We maintain the same w distribution and calculate the distribution
175 of rain in the warmed climate. The difference between the distributions of rain frequency and
176 amount in the warmed and initial climates are shown in Fig. 4a-c. There is no change in the total
177 frequency of rain, and the total amount of rainfall increases by $7\% \text{ K}^{-1}$, exactly following the
178 change in moisture.

179 The rainfall distribution response to warming is equivalent to moving the rain frequency distri-
180 bution to the right by exactly $7\% \text{ K}^{-1}$, or having equal shift and increase modes of $7\% \text{ K}^{-1}$ (the
181 fitted shift and increase modes are listed in Table 2), as in Fig. 2e,f. In contrast to this warming
182 experiment, in climate model simulations of global warming, the shift mode is larger than in the
183 increase mode and total precipitation increases more slowly than moisture. This exposes a flaw:
184 circulation also adjusts to changes in climate, which is not captured by this first experiment. In
185 climate model projections, circulation adjusts to satisfy the energetic constraints of the climate
186 system, including the constraint that precipitation (in the global mean) can only increase as much
187 as atmospheric radiative cooling and sensible heat flux allow it to (e.g. Allen and Ingram 2002).

188 *c. Response to weakening circulation*

189 A weakening of the atmospheric overturning circulation can be effected in our model by reduc-
190 ing the width of the vertical velocity distribution, σ_w . For our second experiment, we decrease
191 the standard deviation of w by 4%, using the initial (not warmed) distribution of temperature and
192 moisture. The change in the distribution of rain is shown in Fig. 4d-f.

193 Again, there is no change in the dry frequency, and the total amount of rainfall decreases by 4%,
194 the same amount that we weakened the width of the vertical velocity distribution by. Decreasing
195 the width of the vertical velocity distribution results in a shift of the rain frequency distribution to
196 lower rain rates. In fact, narrowing the w distribution by 7% would exactly cancel the effect of
197 warming by 1 K. We can understand this by considering Eqn. 2 or 3: warming by 1 K increases q
198 by 7%, whereas widening the vertical velocity distribution increases w by 7%. The effect of either
199 change on r is the same.

200 We have just seen that neither warming nor changing the strength of the circulation affects the
201 dry frequency, or the symmetry between the rates of change of mean and extreme rainfall. Changes

202 analogous to those we see in climate model simulations thus cannot result from either warming
203 at constant relative humidity or weakening circulation alone. But what if the circulation becomes
204 more asymmetric?

205 *d. Response to changing skewness of vertical velocity*

206 The first moment of the vertical velocity distribution, its mean, must be fixed at zero to maintain
207 mass conservation. We have just seen that changing the second moment (standard deviation or
208 variance) does not cause the changes in the distribution of rain that we see in climate models.
209 We now turn to the third moment, skewness, which measures the asymmetry of a distribution.
210 Skewness, a key quantity, is attended to more widely in the parts of atmospheric sciences dealing
211 with turbulence, like boundary layer meteorology. It has also received some limited attention in
212 climate recently. Sardeshmukh and Sura (2009) examine how skewness in fields like vorticity can
213 arise. Luxford and Woollings (2012) discuss how skewness arises in geopotential height from
214 kinematic fluctuations of the jet stream. Monahan (2004) discusses skewness of low-level wind
215 speed arising from surface drag.

216 Skewness can arise in vertical motion from the asymmetric effect of latent heating. To visualize
217 this effect, picture a developing thunderstorm. The cumulus cloud grows because an updraft is
218 heated when water vapor condenses, sustaining or even strengthening the updraft and eventually
219 resulting in rainfall. Over the life of the thunderstorm, some of this rainfall will re-evaporate, but
220 there will be a net latent heating of the atmosphere due to the formation of this thunderstorm equal
221 to the amount of rainfall that reaches the ground. There is no corresponding effect of latent heating
222 on subsiding air; it merely warms adiabatically as it sinks.

223 To incorporate skewness into the vertical velocity distribution, we draw w from a skew-normal
224 distribution generated following Azzalini and Capitanio (1999), instead of from a normal distri-

225 bution as before. A skew-normal distribution has three degrees of freedom which determine its
226 mean, variance, and asymmetry. When the asymmetry is zero, the skew-normal distribution be-
227 comes normal. We adjust the skew-normal distribution so that the mean is always zero to maintain
228 mass conservation, and we maintain a constant variance of the w distribution to eliminate the ef-
229 fects of changing circulation strength. The resulting distribution of w and the response in rain
230 frequency and amount distributions to a 0.2 increase in skewness are shown in Fig. 4g-i.

231 The responses of the rain frequency and amount distributions to increasing skewness of the
232 vertical velocity have some intriguing features. There is a notable decrease in the frequency of
233 rain for moderate rain rates (Fig. 4h), but the total amount of rain remains essentially constant due
234 to a slight increase in the frequency of higher rain rates (Fig. 4i). This strongly resembles the shift
235 mode. The magnitude of the strongest updrafts also changes little. Increasing skewness without
236 conserving the mean of w would increase the strength of the strongest updrafts, but the shift of the
237 distribution to maintain mass continuity compensates for this.

238 To move toward the response of precipitation to global warming in climate models, we simul-
239 taneously warm and increase the skewness of the vertical velocity distribution, shown in Fig. 4j-l.
240 The response of the rain frequency and amount distributions to warming and skewing has all the
241 features seen in climate models: a decrease in the total rain frequency and in the frequency of
242 rain falling at moderate rain rates, along with an increase in rain amount focused at the heaviest
243 rain rates. Increasing the skewness of the vertical velocity distribution effects crucial components
244 of the change. It decreases the total frequency of rain events, breaks the symmetry between the
245 changes in mean and extreme rainfall, and allows us to change the magnitude of the shift mode
246 without changing the increase mode.

247 To fully capture the changes we see in climate model simulations, we weaken the distribution
248 of vertical velocity (decrease σ_w) while simultaneously increasing its skewness and increasing \bar{T} ,

249 shown in Fig. 4m-o. Here we see many of the same features as before, but now we also have the
250 decrease in mean rainfall that arises from the weakening circulation, giving us shift and increase
251 modes of roughly the same magnitude as we see in climate models.

252 To recap, we have shown that warming (increasing \bar{T}) results in shift and increase modes of equal
253 magnitude, while increasing the skewness of the vertical velocity distribution produces the shift
254 mode alone, allowing us to reproduce some salient features of the response of the rain distribution
255 to warming projected by climate models. This motivates us to construct a model that predicts ver-
256 tical velocity to understand how atmospheric energetic constraints lead to the increasing skewness
257 of the vertical velocity distribution with warming.

258 **3. The second model: Predicted vertical velocity**

259 We know that precipitation is energetically constrained by total column heating and cooling.
260 Thus, in this model we start with energetics. We prescribe a distribution of non-latent heating
261 Q_n , which is the sum of radiative and sensible heating and the convergence of dry static energy
262 flux in the atmospheric column (see Muller and O’Gorman 2011). In the time mean, \bar{Q}_n balances
263 the latent heating, and so relates to the total precipitation. In daily fields from the MPI-ESM-
264 LR climate model, the width of the atmospheric radiative cooling is small compared to width
265 of the atmospheric column dry static static energy flux convergence distribution, so the standard
266 deviation of the non-latent heating distribution, σ_{Q_n} , comes primarily from the convergence of the
267 dry static energy flux. The distribution of \bar{Q}_n thus captures both the impact of radiation and the
268 transport of energy by the circulation.

269 *a. Model description*

270 Our goal is to predict the distribution of w , which will in turn give us the rainfall from Eqn. 2,
271 as in our first model. We begin with the temperature and moisture distributions (again connected
272 by the assumption of saturation, Fig. 5a), except that the tail of the temperature distribution is
273 truncated at a maximum temperature, T_{max} , which in turn implies a maximum allowable moisture
274 content. We then assume that the non-latent atmospheric column heating, Q_n (Fig. 5b), can be de-
275 scribed by another independent Gaussian distribution. The sum of non-latent atmospheric column
276 heating and latent heating from precipitation must be zero in the time mean to maintain energy
277 conservation.

278 We calculate the distributions of vertical velocity and rain according to a form of the thermody-
279 namic equation (inspired by Sobel and Bretherton 2000),

$$wS = Q_n + Q_l, \quad (5)$$

280 where the parameter S is a constant that converts energy to vertical motion. In Sobel and Brether-
281 ton (2000), S is a stability that varies in time and space, but here we assume it is a constant to
282 maintain the mathematical simplicity of the model. Physically, this equation implies that the total
283 atmospheric column heating (both latent, Q_l , and non-latent Q_n) exactly balances the energy re-
284 quired to move air (w) against stability S . This balance holds in the time mean in the real world,
285 but here we enforce it at all times.

286 We calculate the latent heating Q_l from the moisture and vertical velocity when it is raining (as
287 in the first model),

$$Q_l = L\rho_a wq, \quad (6)$$

288 where L is the latent heat of vaporization of water (which we hold constant at 2.5×10^6 J kg⁻¹, its
289 value at 0°C) and ρ_a is the air density as in the first model. With substitution, we have an equation

290 for vertical velocity,

$$w = \begin{cases} \frac{Q_n}{S}, & Q_n \leq 0 \\ \frac{Q_n}{S - L\rho_a q}, & Q_n > 0. \end{cases} \quad (7)$$

291 To conserve mass, the average vertical velocity must equal zero, as in the first model, and to con-
292 serve energy, the mean latent heating Q_l must be equal and opposite to the mean non-latent heating
293 Q_n . These balances are effected by integral constraints based on Eqn. 5, derived in Appendix B.

294 The parameters we use are listed in Table 3. The mean of the non-latent atmospheric column
295 heating is equal but opposite to the CMIP5 multi-model mean precipitation (88 W m^{-2}), and its
296 standard deviation is dominated by variability in the dry static energy flux convergence on short
297 time scales (following Muller and O’Gorman 2011); we choose a value similar to those we found
298 in climate model integrations.

299 Truncating the temperature distribution is necessary to ensure that the denominator in Eqn. 7
300 never drops to or below zero, which would result in infinite w . T_{max} can be interpreted as an upper
301 bound on SST, which is enforced by convection in the real world (Sud et al. 1999; Williams et al.
302 2009).

303 In addition to our choice of $\overline{Q_n}$, we also choose \overline{T} , σ_T , T_{max} , and σ_{Q_n} values that are plausibly
304 realistic or comparable to calculations using daily data from the MPI-ESM-LR climate model. The
305 other requirement to maintain a positive-definite denominator in Eqn. 7 is that S must be greater
306 than $L\rho_a q(T_{max})$. In this way, the minimum possible choice of the parameter S is tied to T_{max} . With
307 a realistic temperature and moisture distribution and a constant S , the minimum allowable value
308 of S is much larger than observed values of static stability (see e.g., Jukes 2000).

309 The distributions of vertical velocity and rain produced by our model with the parameters listed
310 in Table 3 are shown in Fig. 5c-e. As with the first model, the distributions of rain frequency and

311 amount are qualitatively similar to observations and climate model simulations in terms of both
312 the peak magnitudes and overall structure.

313 Most importantly, the model predicts a skewed distribution of w . To ensure that the skewness
314 was not an artifact of the non-zero mean of the non-latent heating distribution, we specified $\bar{Q}_n = 0$
315 (thereby neglecting energy and mass balance) in an alternative calculation (not shown), and the
316 positive skewness remained. Rather, the skewness arises from the asymmetry introduced by latent
317 heating, as can be seen in Eqn. (7). Atmospheric column cooling ($Q_n < 0$) causes downward
318 velocity, with a magnitude linearly related to Q_n , since S is constant. But atmospheric heating
319 ($Q_n > 0$) induces upward motion and also condensation. The resulting latent heating effectively
320 weakens the stability. w is thus no longer simply proportional to Q_n , but grows super-linearly with
321 Q_n .

322 *b. Perturbations about the control climate*

323 Here we explore the responses to the three parameters other than warming: mean non-latent
324 heating \bar{Q}_n , the width of non-latent heating σ_{Q_n} , and stability S . To maintain mass and energy
325 conservation, when one parameter changes, it must be compensated by a change in at least one
326 other parameter. The amplitude of the parameter changes described in this section were chosen so
327 they can be compared with the next set of experiments, where we warm by 3 K. This is a fairly
328 linear regime where the results are not highly sensitive to the amplitude of the perturbations.

329 In the first experiment, we increase the magnitude of mean non-latent heating \bar{Q}_n by 24 W m^{-2}
330 to 113 W m^{-2} and balance it by widening the non-latent heating distribution (allowing σ_{Q_n} to
331 increase by 27.5%, equivalent to increasing the strength of heat transport convergence). Details
332 of how we carry out the variation of the parameters are discussed in Appendix A. The resulting
333 distribution of vertical velocity and the changes in rain amount and rain frequency are shown in

334 Fig. 6a-c. The vertical velocity distribution has widened, with no change in skewness. The rain
335 frequency distribution shifts to heavier rain rates, with no change in the dry frequency, and thus
336 no change in total rain frequency. The total amount of rainfall increases (to balance the increase
337 in magnitude of non-latent heating), reflected in the response of the rain amount distribution.

338 Also included in Fig. 6c is the combined shift-plus-increase mode fitted to the rain amount
339 response. The fitted shift-plus-increase response is colored orange (following the color scheme
340 shown in Fig. 2), which corresponds to equal magnitudes of shift and increase modes. The magni-
341 tudes and error of the fit are listed in Table 2 (and are normalized by 3 K warming to compare with
342 warming experiments, discussed next); the error is the magnitude of the response that the fitted
343 shift-plus-increase fails to capture. The fitted shift mode is slightly bigger than the fitted increase
344 mode, 11 versus 9 % K^{-1} .

345 The response of the vertical velocity and rainfall distributions is essentially the same response
346 we would get from strengthening w in the first model (the opposite of the weakening w experiment
347 in Fig. 4d-f), only here it is achieved in a way that is consistent with energy as well as mass
348 balance. In this experiment, the magnitudes of vertical velocity and rain change, but the shape of
349 their distributions, including of the fraction of events that are rain-producing updrafts, does not.

350 In the second experiment, we again increase the magnitude of mean non-latent heating, but now
351 hold the width of the non-latent heating distribution constant and instead decrease stability S . We
352 determine the decrease in S required to balance the increase in \bar{Q}_n by linearizing the energy/mass
353 balance equation about a perturbation in S , shown in Appendix C. A decrease of S by 19% is
354 needed to maintain balance, as shown in Fig. 6d-f. Again we see strengthening of the vertical
355 velocity distribution, but here we also see an increase in skewness of 38%. The change in rain
356 frequency distribution has a shape that is similar to but not the same as in the previous experiment,
357 because the symmetry is broken: there is an increase in the dry-day frequency by 0.4%, and thus

358 a decrease in the total rain frequency. This change in symmetry arises from changing the mean of
359 Q_n without changing its width, so that the fraction of non-latent heating events that are positive
360 decreases (the positive w events and rainfall follow). The fitted shift-plus-increase mode to the
361 rain amount response is colored magenta to correspond to a broken symmetry between the shift
362 and increase modes.

363 In the third experiment, we narrow the distribution of non-latent heating by decreasing σ_{Q_n} by
364 23% and compensate it by decreasing S by 20%, holding \bar{Q}_n constant (Fig. 6g-i). Here, there
365 is negligible change in the width, or strength, of the vertical velocity distribution, but there is an
366 increase in skewness which arises from strong (though still relatively infrequent) updrafts. The dry
367 frequency increases, so there is an overall decrease in rain frequency, occurring mainly at moderate
368 rain rates. At the same time, there is a slight increase in frequency at the heaviest rain rates and
369 a larger (but still small) increase at light rain rates. The response of the rain amount distribution
370 is dominated by the decrease at moderate rain rates and increase at heavy rain rates, which are in
371 balance because the total rainfall does not change (\bar{Q}_n is fixed). The shift-plus-increase mode is
372 not a good fit for this response (light gray represents a poor fit of the shift-plus-increase mode).

373 The response of the vertical velocity distribution is a negligible change in width but an increase
374 in skewness, which we can understand as follows. The narrowing Q_n distribution would weaken
375 the vertical velocity distribution, but this is countered by the decrease in S which strengthens it (see
376 Eqn. 7). Meanwhile, decreasing σ_{Q_n} with no corresponding change in \bar{Q}_n decreases the fraction
377 of events that are updrafts. The w distribution must adjust so that the same total latent heating is
378 achieved through fewer updrafts, which is accomplished by strengthening the strongest updrafts,
379 increasing the skewness of vertical velocity.

380 The response of the rain frequency and amount distributions to changing σ_{Q_n} and S in Fig. 6g-i
381 has some similarities to but also differences from the response to increasing skewness of w in the

382 first model (Fig. 4g-i). The close fit by the shift mode of the rain amount response to increasing
383 skewness in the first model indicates that the response is mostly just a movement of the rain amount
384 distribution to higher rain rates. In contrast, in this model and experiment, the shift mode poorly
385 captures the response. Despite that it is not captured by the shift and increase modes, the rain
386 frequency and amount responses have interesting resemblances to the global warming response in
387 climate models. One feature present here and in climate models that is not captured by the shift-
388 plus-increase is the light rain mode identified in Pendergrass and Hartmann (2014b). The light
389 rain mode is the small increase at light rain rates (around 1 mm d^{-1}) visible in Fig. 1c.

390 To summarize the effect of perturbing parameters other than temperature in this model: increas-
391 ing \overline{Q}_n increases the total amount of rainfall, while increasing σ_{Q_n} and decreasing S increase the
392 magnitude of vertical velocity events and the intensity of rainfall. When the combination of pa-
393 rameters changes in such a way that the fraction of events that are updrafts changes, the skewness
394 of the vertical velocity distribution also changes.

395 *c. Response to warming*

396 Next, we explore the response of the vertical velocity and rainfall distributions to warming. We
397 increase \overline{T} by 3 K (while allowing T_{max} to increase by the same amount). To maintain energy and
398 mass balance while warming, we will begin by adjusting one other parameter at a time, considering
399 three experiments in turn, shown in Fig. 7.

400 In the first experiment, we balance warming by increasing S . Stability also changes in climate
401 model simulations of global warming; specifically, dry static stability increases with warming in
402 the midlatitudes and subtropics (Frierson 2006; Lu et al. 2007). We determine effects of changing
403 T on energy and mass balance and the increase in S needed to balance it by linearizing Eqn. B4 for
404 energy and mass balance about perturbations in S and T , shown in Appendix C. This linearization

405 shows that a degree of warming is balanced by a 7% increase in stability, where the factor of 7%
406 arises from the moistening associated with the warming. The distributions of vertical velocity and
407 moisture that result from warming by 3 K and increasing stability by 21% are shown in Fig. 7a-c.
408 The increased stability decreases the magnitude of vertical velocity for a given atmospheric col-
409 umn heating, so that the vertical velocity is weakened (its standard deviation decreases, as in Held
410 and Soden 2006; Vecchi and Soden 2007) and the distribution of rainfall is exactly unchanged.
411 The skewness of vertical velocity is also unchanged. In this model, the dry frequency is just the
412 fraction of the time that the atmospheric column heating is negative; since atmospheric column
413 heating does not change in this experiment, neither does the dry frequency. The tradeoff between
414 warming and stability here is similar to the tradeoff between warming and the width of the vertical
415 velocity distribution in our first model.

416 In the second experiment, we warm while increasing the magnitude of mean non-latent heating
417 \bar{Q}_n and holding all other parameters constant. Recall that \bar{Q}_n controls the total precipitation. The
418 resulting distributions of vertical velocity and rainfall are shown in Fig. 7d-f. The resulting vertical
419 velocity distribution has no substantial change in width, but it does have increase in skewness.
420 Similarly to the “narrow Q_n and decrease S ” experiment in Fig. 6g-i, the increase in moisture and
421 increase in mean Q_n have largely compensating effects on the vertical velocity distribution, except
422 for a decrease in the total fraction of updrafts compared to downdrafts, resulting in an increase
423 in skewness with little change in width of the w distribution. The response of the rain frequency
424 distribution, on the other hand, is more similar to the increasing \bar{Q}_n and decrease S experiment.
425 There is an increase in the dry frequency, and the rain amount response is captured by a shift mode
426 that is slightly larger than the increase mode. Examination of Eqns. 2 and 7 reveals that this is
427 possible because both experiments have the same change in Q_n , and decreasing S has the same
428 effect on the denominator of Eqn. 7 as increasing q .

429 In the third experiment, warming is balanced by narrowing of the non-latent heating distribution
430 (decreasing σ_{Q_n} or weakening the dry static energy flux convergence, Fig. 7g-i). In this exper-
431 iment, the vertical velocity distribution weakens while the skewness increases. The skewness
432 arises because of the decrease in upward frequency and adjustments to maintain mass as well
433 as energy balance, while the weakening results from the weakening of the Q_n distribution. The
434 rain frequency and amount distributions are very similar to the “narrowing Q_n and decreasing S ”
435 experiment with no warming.

436 In two final experiments, we emulate the changes seen in climate models: we warm and also
437 increase the magnitude of non-latent atmospheric column heating \bar{Q}_n by $1.1 \text{ W m}^{-2} \text{ K}^{-1}$, which
438 is the rate at which global-mean precipitation and clear-sky atmospheric radiative cooling increase
439 in climate model projections of the response to transient carbon dioxide increase (Pendergrass and
440 Hartmann 2014a). This change in atmospheric radiative cooling includes both the temperature-
441 mediated and direct effects of carbon dioxide. To maintain mass and energy balance, we allow
442 a third parameter to change, and keep the fourth constant (first increasing S , and then decreasing
443 σ_{Q_n}); these experiments are shown in Fig. 8. We examine each parameter change separately, but
444 in at least one climate model simulation forced by a transient increase in carbon dioxide (with the
445 MPI-ESM-LR model) both of changes occur: S increases (by 1.7 \% K^{-1}) and σ_{Q_n} decreases (by
446 0.7 \% K^{-1}).

447 First, we warm, increase mean Q_n , and allow S to increase. According to the linearizations
448 about S and T in Appendix C, a change in stability of 6.0 \% K^{-1} is needed to maintain energy
449 and mass balance. The result (shown in Fig. 8a-c) is a combination of the experiments where we
450 warmed and varied mean Q_n and S separately. The vertical velocity distribution weakens and has
451 a small increase in skewness. There is a modest increase in dry frequency, and a modest break in

452 symmetry between the shift and increase modes (2.0 versus 1.6 % K^{-1}). This is not as large as the
453 break in symmetry we see in climate models.

454 Finally, we warm, increase mean Q_n , and allow σ_{Q_n} to decrease by 6.2 % K^{-1} . In Fig. 8d we see
455 a weakening of the vertical velocity distribution and a larger increase in skewness than in Fig. 8a.
456 Analogously to the warming and skewing experiment with the first model, the rain frequency
457 and amount distribution responses (Fig. 8e,f) resemble the superposition of responses in previous
458 experiments. The dry frequency increases, and the response of the rain frequency distribution has
459 a decrease at moderate rain rates that is partially compensated by an increase at heavy rain rates.
460 The rain frequency response strongly resembles the response we see in climate models (Fig. 1c),
461 except that the light rain mode is absent. The rain amount distribution response is partially but not
462 completely captured by the shift and increase modes, which reflects that it is the sum of a response
463 that the shift-plus-increase captures (the response to warming while and increasing $|\overline{Q}_n|$) and one
464 that it does not (the response to changing σ_{Q_n}). The fitted shift-plus-increase overestimates the
465 decrease at moderate rain rates and underestimates the increase at heavy rain rates, reminiscent of
466 the extreme mode identified in Pendergrass and Hartmann (2014b).

467 To summarize, in our second model, the atmosphere can respond in three ways to warming: (1)
468 increasing the stability (S), which weakens the circulation (w) but has no effect on rain, (2) in-
469 creasing the total precipitation (\overline{Q}_n), which drives an increase in skewness of w and of the intensity
470 of the heaviest rainfall events, and (3) decreasing the width of the non-latent heating distribution
471 (σ_{Q_n}), which leads to both a weakening of the circulation and increase in its skewness, and the
472 accompanying increase in intensity of the heaviest rainfall events. In climate model projections of
473 warming, energetic constraints require an increase in the total precipitation \overline{Q}_n .

474 In this simple model, if we warm and increase mean latent heating \overline{Q}_n , the stability S and/or
475 width of the non-latent heating distribution σ_{Q_n} – which is intimately related to the circulation

476 – must also change to maintain energy and mass balance. Any combination of these parameter
477 changes results in: (1) a weakening of the circulations (i.e. of w), the essential conclusion of
478 Vecchi and Soden (2007), (2) an increase in the skewness of w , and (3) an increase in intensity of
479 the heaviest rain events (e.g., Trenberth 1999).

480 **4. Comparison with the response to warming in climate models**

481 The two heuristic models above show that increasing skewness of the vertical velocity distri-
482 bution coincides with key characteristics of the changing distribution of rainfall that we see in
483 climate models. Does skewness of the vertical velocity distribution increase with warming in
484 climate models?

485 To address this question, we calculate statistics of daily-average 500 hPa pressure vertical veloc-
486 ity and their change in three warming experiments in the CMIP5 archive (Table 4). We calculate
487 the area-weighted global-average moments from years 2006-2015 and 2090-2099 in the RCP8.5
488 scenario, and years 1-10 and 61-70 in the transient carbon dioxide increase 1pctCO2 scenario;
489 these results can be compared with the fitted shift-plus-increase modes of the distribution of rain
490 in Pendergrass and Hartmann (2014b). Trends in data can contaminate statistical measures of a dis-
491 tribution, so we also analyze the last 10 years of the CO₂ quadrupling experiment (abrupt4xco2),
492 when the climate is as close to equilibrating as is available in the CMIP5 archive, and trends are
493 as small as possible.

494 All climate model simulations have increasing skewness of vertical velocity, consistent with
495 our expectations from the heuristic models along with the changing distribution of rain in climate
496 models. The magnitude of increase in skewness varies widely across models, from less than 1
497 to 27 % K⁻¹. Note that the models with the biggest increases in skewness (the GFDL-ESM and
498 IPSL-CM5A models) also have a large extreme mode (Pendergrass and Hartmann 2014b). While

499 we have touched on the extreme mode in our second heuristic model, much about it remains to be
500 investigated.

501 The variance of vertical velocity decreases in all but one of the climate model simulations.
502 Decreasing variance of vertical velocity at 500 hPa is consistent with Held and Soden (2006) and
503 Vecchi and Soden (2007), though their metrics were slightly different from ours and the magnitude
504 of changes shown here is smaller. Additionally, the change in vertical velocity strength at 500 hPa
505 is expected to underestimate the weakening of the total vertical overturning circulation because the
506 strongest motion is above 500 hPa and shifts upward with warming (Singh and O’Gorman 2012).

507 We include the changes in kurtosis in Table 4, the fourth moment of the distribution. Larger
508 kurtosis corresponds to a fatter tail and a narrower peak of the distribution; a normal distribution
509 has a kurtosis of 3 (e.g., DeCarlo 1997). In all climate models, kurtosis of vertical velocity is
510 initially greater than gaussian, and it increases with warming. Our second model predicts an
511 increase in kurtosis along with the increases in skewness. Interestingly, the GFDL models have by
512 far the largest increases in kurtosis with warming (they also have large extreme modes).

513 We are now in a position to reconcile the differing magnitudes of the shift and increase modes
514 with warming that we see in climate model simulations. For the multi-model mean, moistening
515 occurs at about 6-7 % K^{-1} and global mean precipitation increases at 1.5 % K^{-1} . The multi-model
516 mean rain amount response has an increase mode of 1 % K^{-1} and a shift mode of 3.3 % K^{-1} . The
517 MPI-ESM-LR model, whose response is best captured by the shift and increase modes, has an
518 increase mode of 1.3 % K^{-1} and a shift mode of 5.7 % K^{-1} .

519 We relate the shift and increase modes to changes in moisture and circulation as follows (and
520 shown in Fig. 4 as well as listed in Table 2): moistening at 7 % K^{-1} results in equal magnitudes
521 of shift and increase modes. This is countered by a narrowing of the vertical velocity distribution
522 that is not quite as large, bringing the net magnitudes of both the shift and increase modes down.

523 Finally, an increase in skewness of the vertical velocity distribution results in a shift mode with no
524 corresponding increase mode. The combination of these three changes results in a shift mode that
525 is larger than the increase mode seen in the climate model response to warming.

526 While the heuristic models developed here capture some important aspects of the response of
527 rainfall and vertical velocity to warming seen in climate models, the cost of its simplicity is the
528 number of assumptions that must be made. Assumptions for our idealized relationship between
529 moisture, vertical velocity and rain rate include: that all moisture is removed whenever there is
530 upward motion, that the vertical structure of the atmosphere is fixed, and that relative humidity
531 does not change. Our models do not accommodate any unresolved processes, parameterized in
532 climate models, which can alter the relationship between rainfall and vertical velocity. This ide-
533 alized framework also does not address the differing direct and temperature-mediated responses
534 of precipitation and circulation to greenhouse gas forcing. Finally, aggregating over all locations
535 and seasons convolves many different processes, and the relationships we explore here may not
536 hold for all of them. Nonetheless, while we anticipate that our heuristic models do not capture the
537 behavior of every relevant process that contributes to the responses of rainfall and vertical velocity
538 to global warming, we think these models are useful for understanding a substantial portion of the
539 response in many regions of most climate models.

540 **5. Convective area**

541 The spatial manifestation of the distribution of rain and vertical velocity is convective area, by
542 which we mean the area with upward motion and the cloudiness and rainfall that accompany it.
543 The fraction of time that vertical motion is upward and the fraction of time that it is raining in
544 the heuristic models presented here is analogous to the fraction of the area in a domain where
545 rain is occurring. The literature is currently unsettled about how the change in convective area

546 and frequency of upward motion are expected to change with warming. Johnson and Xie (2010)
547 argues that the convectively active fractional area of the tropics changes little relative to the area
548 above an absolute SST threshold, which increases by 45% over the 21st century in the experiments
549 they analyze. In contrast, Vecchi and Soden (2007) report a decrease in the number of grid points
550 with upward motion in GFDL-CM2.1 simulations of global warming in the tropics. Other recent
551 studies find a decrease in the area of the ITCZ with warming (Neelin et al. 2003; Huang et al.
552 2013). In CMIP5 model simulations, the frequency of dry days has a small but significant increase
553 (see Fig. 1a or Pendergrass and Hartmann 2014b).

554 The heuristic models shown here reproduce the increase in dry frequency seen in the CMIP5
555 models and thus also the decrease in convective area. Figure 9 shows a schematic of the tropical
556 overturning circulation to aid in interpreting its response to changes in the distribution of vertical
557 velocity. The initial distribution has a region of ascent that is narrower than the region of descent,
558 analogous to the circulation in the tropical atmosphere (Fig. 9a). Because the region of ascent is
559 narrower and mass is conserved, the ascending motions are stronger than corresponding descend-
560 ing ones. Decreasing the standard deviation of the vertical velocity distribution decreases the
561 magnitude of both upward and downward motion (weakening the circulation), with no change in
562 area of either region (Fig. 9b). Increasing the skewness of vertical velocity increases the magnitude
563 of upward motion while decreasing its area, and decreases the speed of descent while increasing
564 its area (Fig. 9c). When the decrease in standard deviation and increasing skewness occur to-
565 gether, both contribute to weakening the descending motion, but they have competing effects on
566 the magnitude of ascent, resulting in little change in updraft strength (Fig. 9d).

567 **6. Conclusion**

568 We have introduced two idealized models relating the distributions of rain and vertical veloc-
569 ity. In both models, temperature (and thus moisture, assuming constant relative humidity) is pre-
570 scribed, and the distribution of rainfall is predicted. In the first model, the distribution of vertical
571 velocity is also prescribed and can be varied; mass conservation is respected. In the second model,
572 the distribution of non-latent atmospheric column heating is prescribed, the distribution of vertical
573 velocity is predicted, and both mass and energy are conserved. Some key assumptions made by
574 both models are that relative humidity is fixed within and between climate states and that stability
575 is constant within each climate state.

576 Both of these models show that increasing skewness, or asymmetry, of the vertical velocity dis-
577 tribution is necessary to recover important characteristics of the changing distribution of rain with
578 warming predicted by climate models: dry-day frequency increases, and extreme precipitation in-
579 creases at a rate faster than the increase in mean precipitation. In the context of shift and increase
580 modes of change of the distribution of rain, an increase in skewness is necessary to achieve the
581 larger shift mode than increase mode seen in climate model projections. The second model, where
582 the distribution of vertical velocity is predicted, shows how the asymmetric influence of latent
583 heating creates skewness in the vertical velocity distribution. Experiments with this model show
584 that this skewness increases in response to warming, along with the adjustments needed to main-
585 tain mass and energy balance. In addition to an increase in skewness, the standard deviation of
586 the vertical velocity distribution also decreases, consistent with the weakening circulation found
587 in climate model simulations of global warming.

588 The models developed here capture salient aspects of the changing distributions of rain and
589 vertical velocity with simple thermodynamic relationships, implying that we do not need to resort

590 to complex dynamical explanations for these aspects of the changing distribution of rain. The
591 idealized relationships between the distributions of vertical velocity and precipitation explored
592 here hopefully form a basis for understanding the richer and more complex interactions in climate
593 models and in the real world.

594 *Acknowledgments.* We thank Clara Deser, Ben Sanderson, Brian Rose, and Flavio Lehner for
595 their feedback. NCAR's Advanced Studies Program postdoctoral research fellowship provided
596 funding for AGP. EPG acknowledges support from the National Science Foundation through grant
597 AGS-1264195.

598 APPENDIX A

599 Numerical solutions

600 *a. Normal and skew-normal distributions*

601 We calculate the value of the normal distribution at points that are evenly spaced in percentile
602 space, 5000 for Model 1 and 10 000 for Model 2. For the temperature distribution, at this point
603 any values of $T > T_{max}$ are truncated. For making calculations over joint distributions (r over T/q
604 and w in Model 1, r and w over Q_n and T/q in Model 2), we form a matrix over both distributions
605 (5000×5000 or $10\,000 \times 10\,000$ ¹) and calculate the value at each point in the joint space.

606 Calculating the skew normal distribution is similar to a joint distribution because the algorithm
607 of Azzalini and Capitanio (1999) calls for operating on two normal distributions. We start with
608 two normal distributions u_0 and v (5000 samples for each). To get a distribution with a shape
609 parameter a (which is related to the skewness; when a is zero the distribution is normal and we use
610 $a > 0$ here), we calculate $u_1 = du_0 + \sqrt{(1 - d^2)}v$, where $d = a/\sqrt{(1 + a^2)}$ is a correlation related

¹With the introduction of T_{max} , we truncate a few values at the high end of the T/q distribution.

611 to the shape parameter. Then, the skewed distribution z is u_1 when $u_0 > 0$, and $-u_1$ otherwise.
612 Finally, this 5000 x 5000 array is subsampled back to 5000 values by sorting the values them and
613 keeping every 5000th value.

614 *b. Frequency and amount distributions*

615 We use logarithmically-spaced bins for the rain frequency and amount distributions, and choose
616 250 of them to obtain stable fits of the shift-plus-increase modes. Details of the calculation and
617 further examples of rain amount and rain frequency distributions can be found in Pendergrass and
618 Hartmann (2014c). We use 50 linearly-spaced bins for $p(T)$, $p(Q_n)$, and $p(w)$, which we use for
619 display only.

620 *c. Model 2 parameters*

621 To calculate the parameters in the second model, there are two steps: the initial set up to find a
622 balanced state, and then allowing parameters to vary about this state.

623 To set up the model initially, the challenge is meeting energy and mass balance; this happens
624 numerically by specifying all parameters other than \bar{Q}_n , and then systematically solving for the
625 value of \bar{Q}_n that achieves energy and mass balance. First, we calculate the distribution of T from
626 \bar{T} and σ_T , truncating anything over T_{max} , and the associated q . Then with a choice of S , we
627 calculate the LHS of the energy/mass balance equation (B). Finally, use a specified value of σ_{Q_n} ,
628 and solve systematically for the value of \bar{Q}_n that most closely results in mass/energy balance. We
629 take a vector of 10 000 gaussian values evenly spaced percentile-wise (call them y), and using
630 the σ_{Q_n} value, calculate the RHS of the energy/mass balance equation that would result for each
631 choice of $\bar{Q}_n = y\sigma_{Q_n}$. New \bar{T} , σ_T , S , and σ_{Q_n} values can be manually chosen and a new \bar{Q}_n found
632 to vary parameters.

633 To find a new balanced state due to small variations in T and S around the initial balanced state,
634 we use the linearizations in Appendix C. This is done in three different ways. Whenever possible,
635 we use the linearization alone to find new values of T and S , or of the new LHS of the energy/mass
636 balance equation. When necessary, we re-solve for a new \bar{Q}_n that best meets energy/mass balance
637 as we did to find the initial balanced \bar{Q}_n value. Otherwise (e.g., changing σ_{Q_n}), we iteratively
638 choose parameter values (manually) until the energy/mass balance equation is satisfied again (to
639 4 decimal places). Once we have a new set of parameters, r , w , and their frequency and amount
640 distributions $p(r)$, $P(r)$, and $p(w)$ are calculated once again.

641 APPENDIX B

642 Conservation of mass and energy

643 In this appendix, we derive the equation for mass and energy conservation of the model described
644 in Section 3. In order to conserve mass, we must maintain an integral of vertical velocity over the
645 entire distribution equal to zero,

$$\int_{-\infty}^{\infty} \int_0^{q_{max}} w p(q, Q_n) dq dQ_n = 0, \quad (\text{B1})$$

646 where $p(q, Q_n)$ is the joint probability distribution function (pdf) of q and Q_n , and q_{max} is the
647 maximum realized specific humidity, occurring at temperature T_{max} . In order to conserve energy,
648 we enforce that the total latent heating must be balanced by the total non-latent heating,

$$\int_{-\infty}^{\infty} Q_n p(Q_n) dQ_n + \int_{-\infty}^{\infty} \int_0^{q_{max}} L r p(q, Q_n) dq dQ_n = 0, \quad (\text{B2})$$

649 where $p(Q_n)$ is the pdf of non-latent heating Q_n .

650 Substituting Eqns. 2 and 5 into B2, separating regions of positive and negative Q_n , exploiting
 651 the independence of q and Q_n , and rearranging, we have,

$$\int_0^{q_{max}} \left[\frac{1}{1 - L\rho_a q/S} \right] p(q) dq = \frac{-\int_{-\infty}^0 Q_n p(Q_n) dQ_n}{\int_0^{\infty} Q_n p(Q_n) dQ_n}. \quad (\text{B3})$$

652 It is also possible to arrive at Eqn. B3 by starting from the mass conservation constraint
 653 (Eqn. B1), substituting Eqn. 5, exploiting the independence of q and Q_n , recognizing that
 654 $\int p(q) dq = 1$, and rearranging.

655 Following either path, we find that both the mass and energy constraints are met when,

$$E_q \left[\frac{1}{1 - L\rho_a q/S} \right] = \frac{-\int_{-\infty}^0 Q_n p(Q_n) dQ_n}{\int_0^{\infty} Q_n p(Q_n) dQ_n}, \quad (\text{B4})$$

656 where the expectation operator is defined as $E_x[f(x)] = \int_{-\infty}^{\infty} f(x)p(x)dx$.

657 APPENDIX C

658 **Linearization of energy and mass balance about T and S**

659 Here, we linearize the mass and energy conservation equation about its base state (the left hand
 660 side of Eqn. B4) to obtain its response to small changes in stability S and mean temperature \bar{T} .
 661 Along with new values of \bar{Q}_n and σ_{Q_n} chosen by trial and error, we use this linearization to find new
 662 sets of parameters that satisfy energy and mass balance in the experiments described in Section
 663 3c. To be concise, in this appendix we refer to the LHS of Eqn. B4 as B ,

$$B = E_T \left[\frac{1}{1 - L\rho_a q(T)/S} \right]. \quad (\text{C1})$$

664 *a. Linearization in T*

665 First, we linearize the LHS of Eqn. B4 to find its response to small changes in \bar{T} and the asso-
 666 ciated moistening. We expand $T = \bar{T} + \Delta T = \bar{T}(1 + x)$, where $x = \Delta T/\bar{T} \ll 1$. Incorporating our

667 moisture equation (1), we have,

$$B = \int_{-\infty}^{T_{max}} \frac{1}{1 - L\rho_a q_0 e^{0.07\bar{T}(1+x)}/S} p(T) dT. \quad (C2)$$

668 A first order Taylor expansion around B gives us,

$$B \approx B_0 + 0.07 \Delta T B_1, \quad (C3)$$

669 where B_0 is the value of B evaluated at $T = \bar{T}$ and,

$$B_1 \equiv \int_0^{q_{max}} \frac{L\rho_a q/\bar{S}}{(1 - L\rho_a q/\bar{S})^2} p(q) dq. \quad (C4)$$

670 This integral is readily evaluated numerically from a base q distribution.

671 *b. Linearization in S*

672 Next, we linearize Eqn. B4 to find the response to small changes in stability S . Expanding

673 $S = \bar{S} + \Delta S = \bar{S}(1+x)$, where $x = \Delta S/\bar{S} \ll 1$, we have,

$$B = \int_0^{q_{max}} \frac{1}{1 - L\rho_a q/\bar{S}(1+x)} p(q) dq. \quad (C5)$$

674 Another Taylor expansion gives us,

$$B \approx B_0 - \frac{\Delta S}{\bar{S}} B_1. \quad (C6)$$

675 We can combine Eqns. C3 and C6 and solve for ΔS ,

$$\Delta S = S \left(0.07 \Delta T - \frac{B - B_0}{B_1} \right). \quad (C7)$$

676 Given a ΔT and possibly a new value of \bar{Q}_n or σ_{Q_n} (which requires calculating a new value of B),

677 we can solve for the ΔS that satisfies mass and energy balance.

678 **References**

679 Allen, M. R., and W. J. Ingram, 2002: Constraints on future changes in climate and the hydrologic
680 cycle. *Nature*, **419 (6903)**, 224–232, doi:10.1038/nature01092.

681 Azzalini, A., and A. Capitanio, 1999: Statistical applications of the multivariate skew normal
682 distribution. *Journal of the Royal Statistical Society: Series B (Statistical Methodology)*, **61** (3),
683 579–602, doi:10.1111/1467-9868.00194.

684 Betts, A. K., 1998: Climate-convection feedbacks: Some further issues. *Clim. Change*, **39** (1),
685 35–38, doi:10.1023/A:1005323805826.

686 Chou, C., C.-A. Chen, P.-H. Tan, and K. T. Chen, 2012: Mechanisms for global warm-
687 ing impacts on precipitation frequency and intensity. *J. Climate*, **25** (9), 3291–3306, doi:
688 10.1175/JCLI-D-11-00239.1.

689 DeCarlo, L. T., 1997: On the meaning and use of kurtosis. *Psychological methods*, **2** (3), 292,
690 doi:10.1037/1082-989X.2.3.292.

691 Emori, S., and S. Brown, 2005: Dynamic and thermodynamic changes in mean and extreme
692 precipitation under changed climate. *Geophys. Res. Lett.*, **32** (17), L17706, doi:10.1029/
693 2005GL023272.

694 Frierson, D. M., 2006: Robust increases in midlatitude static stability in simulations of global
695 warming. *Geophys. Res. Lett.*, **33** (24), doi:10.1029/2006GL027504.

696 Held, I. M., and B. J. Soden, 2006: Robust responses of the hydrological cycle to global warming.
697 *J. Climate*, **19** (21), 5686–5699, doi:10.1175/JCLI3990.1.

698 Huang, P., S.-P. Xie, K. Hu, G. Huang, and R. Huang, 2013: Patterns of the seasonal response of
699 tropical rainfall to global warming. *Nat. Geosci.*, **6** (5), 357–361, doi:10.1038/ngeo1792.

700 Johnson, N. C., and S.-P. Xie, 2010: Changes in the sea surface temperature threshold for tropical
701 convection. *Nat. Geosci.*, **3** (12), 842–845, doi:10.1038/ngeo1008.

- 702 Juckes, M., 2000: The static stability of the midlatitude troposphere: The relevance of moisture.
703 *J. Atmos. Sci.*, **57 (18)**, 3050–3057.
- 704 Lau, W. K.-M., H.-T. Wu, and K.-M. Kim, 2013: A canonical response of precipitation char-
705 acteristics to global warming from CMIP5 models. *Geophys. Res. Lett.*, **40 (12)**, 3163–3169,
706 doi:10.1002/grl.50420.
- 707 Lu, J., G. A. Vecchi, and T. Reichler, 2007: Expansion of the Hadley cell under global warming.
708 *Geophys. Res. Lett.*, **34 (6)**, doi:10.1029/2006GL028443.
- 709 Luxford, F., and T. Woollings, 2012: A simple kinematic source of skewness in atmospheric flow
710 fields. *J. Atmos. Sci.*, **69 (2)**, 578–590, doi:10.1175/JAS-D-11-089.1.
- 711 Monahan, A. H., 2004: A simple model for the skewness of global sea surface winds. *J. Atmos.*
712 *Sci.*, **61 (16)**, 2037–2049.
- 713 Muller, C. J., and P. A. O’Gorman, 2011: An energetic perspective on the regional response of pre-
714 cipitation to climate change. *Nat. Climate Change*, **1 (5)**, 266–271, doi:10.1038/nclimate1169.
- 715 Neelin, J., C. Chou, and H. Su, 2003: Tropical drought regions in global warming and El Niño
716 teleconnections. *Geophys. Res. Lett.*, **30 (24)**, doi:10.1029/2003GL018625.
- 717 O’Gorman, P. A., R. P. Allan, M. P. Byrne, and M. Previdi, 2012: Energetic constraints
718 on precipitation under climate change. *Surv. Geophys.*, **33 (3-4)**, 585–608, doi:10.1007/
719 s10712-011-9159-6.
- 720 O’Gorman, P. A., and T. Schneider, 2009: The physical basis for increases in precipitation ex-
721 tremes in simulations of 21st-century climate change. *Proc. Natl. Acad. Sci. U. S. A.*, **106 (35)**,
722 14 773–14 777, doi:10.1073/pnas.0907610106.

- 723 Pendergrass, A., and D. Hartmann, 2014a: The atmospheric energy constraint on global-mean
724 precipitation change. *J. Climate*, doi:JCLI-D-13-00163.1.
- 725 Pendergrass, A., and D. Hartmann, 2014b: Changes in the distribution of rain frequency
726 and intensity in response to global warming. *J. Climate*, **27 (22)**, 8372–8383, doi:10.1175/
727 JCLI-D-14-00183.1.
- 728 Pendergrass, A., and D. Hartmann, 2014c: Two modes of change of the distribution of rain. *J.*
729 *Climate*, **27 (22)**, 8357–8371, doi:10.1175/JCLI-D-14-00182.1.
- 730 Romps, D. M., 2014: An analytical model for tropical relative humidity. *J. Climate*, **27 (19)**,
731 7432–7449, doi:10.1175/JCLI-D-14-00255.1.
- 732 Sardeshmukh, P. D., and P. Sura, 2009: Reconciling non-gaussian climate statistics with linear
733 dynamics. *J. Climate*, **22 (5)**, 1193–1207, doi:10.1175/2008JCLI2358.1.
- 734 Singh, M. S., and P. A. O’Gorman, 2012: Upward shift of the atmospheric general circulation
735 under global warming: Theory and simulations. *J. Climate*, **25 (23)**, 8259–8276, doi:10.1175/
736 JCLI-D-11-00699.1.
- 737 Sobel, A. H., and C. S. Bretherton, 2000: Modeling tropical precipitation in a single column. *J.*
738 *Climate*, **13 (24)**, 4378–4392.
- 739 Sud, Y., G. Walker, and K. Lau, 1999: Mechanisms regulating sea-surface temperatures and deep
740 convection in the tropics. *Geophys. Res. Lett.*, **26 (8)**, 1019–1022.
- 741 Taylor, K. E., R. J. Stouffer, and G. A. Meehl, 2012: An overview of CMIP5 and the experiment
742 design. *Bull. Amer. Meteor. Soc.*, **93 (4)**, 485–498, doi:10.1175/BAMS-D-11-00094.1.
- 743 Trenberth, K. E., 1999: Conceptual framework for changes of extremes of the hydrological cycle
744 with climate change. *Wea. Clim. Extremes*, 327–339, doi:10.1007/978-94-015-9265-9_18.

745 Vecchi, G. A., and B. J. Soden, 2007: Global warming and the weakening of the tropical circula-
746 tion. *J. Climate*, **20** (17), 4316–4340, doi:10.1175/JCLI4258.1.

747 Williams, I. N., R. T. Pierrehumbert, and M. Huber, 2009: Global warming, convective threshold
748 and false thermostats. *Geophys. Res. Lett.*, **36** (21), doi:10.1029/2009GL039849.

749 **LIST OF TABLES**

750 **Table 1.** Initial parameter choices for the first model. 38

751 **Table 2.** The magnitude of fitted shift and increase modes along with their error (the
752 magnitude of the response that the fitted shift-plus-increase fails to capture) for
753 each of the experiments shown and discussed here. The precipitation response
754 to a transient CO₂ increase in climate models is shown for the CMIP5 multi-
755 model mean as well as for one GCM (Global Climate Model), MPI-ESM-LR,
756 which is fit the best of all the CMIP5 models (see Pendergrass and Hartmann
757 2014b for details). The Model 1 experiments are shown in Fig. 4 and discussed
758 in Section 2b. Model 2 experiments are shown in Figs. 6-8 and discussed in
759 Section 3c. 39

760 **Table 3.** Initial parameter choices for the second model. 40

761 **Table 4.** Standard deviation, skewness, and kurtosis of 500 hPa pressure vertical veloc-
762 ity from CMIP5 models and their response to warming (normalized by global
763 mean surface temperature change). 41

TABLE 1. Initial parameter choices for the first model.

Variable	Value	Description
\bar{T}	287 K	Mean temperature
σ_T	16 K	Width of temperature dist.
\bar{w}	0	Mean vertical velocity, w
σ_w	1 mm s ⁻¹	Width of w dist.

764 TABLE 2. The magnitude of fitted shift and increase modes along with their error (the magnitude of the
765 response that the fitted shift-plus-increase fails to capture) for each of the experiments shown and discussed
766 here. The precipitation response to a transient CO₂ increase in climate models is shown for the CMIP5 multi-
767 model mean as well as for one GCM (Global Climate Model), MPI-ESM-LR, which is fit the best of all the
768 CMIP5 models (see Pendergrass and Hartmann 2014b for details). The Model 1 experiments are shown in
769 Fig. 4 and discussed in Section 2b. Model 2 experiments are shown in Figs. 6-8 and discussed in Section 3c.

Model	Experiment	Shift (% K ⁻¹)	Increase (% K ⁻¹)	Error (%)
CMIP5 MMM	2xCO ₂	3.3	0.9	33
MPI-ESM-LR	2xCO ₂	5.7	1.3	14
Model 1	Warm	7	7	2
	Weaken w	-4	-4	1
	Skew w	5	-1	27
	Warm, skew w	13	6	15
	Warm, weaken w , skew w	8	2	21
Model 2	Increase \bar{Q}_n , widen Q_n	11	9	11
	Increase \bar{Q}_n , decrease S	11	8	23
	Narrow Q_n , decrease S	0	-1	81
	Warm, increase S	0	0	22
	Warm, increase \bar{Q}_n	11	8	23
	Warm, narrow Q_n	0	-1	81
	Warm, GCM \bar{Q}_n , increase S	2.0	1.6	12
	Warm, GCM \bar{Q}_n , narrow Q_n	1.7	0.5	68

TABLE 3. Initial parameter choices for the second model.

Variable	Value	Description
\bar{T}	287 K	Mean temperature
σ_T	10 K	Width of temperature dist.
T_{max}	317 K	Cap on the temperature dist.
\bar{Q}_n	-88 W m^{-2}	Mean non-latent heating
σ_{Q_n}	$2,500 \text{ W m}^{-2}$	Width of non-latent heating dist.
S	$4.75 \times 10^5 \text{ kg m}^{-1} \text{ s}^{-2}$	Stability

770 TABLE 4. Standard deviation, skewness, and kurtosis of 500 hPa pressure vertical velocity from CMIP5
 771 models and their response to warming (normalized by global mean surface temperature change).

Model	std (Pa s ⁻¹)	Δ std (% K ⁻¹)	skew	Δ skew (% K ⁻¹)	kurtosis	Δ kurtosis (% K ⁻¹)
RCP8.5						
MIROC-ESM-CHEM	9.0	-2.5 %	-0.66	0.57%	5.8	0.85%
FGOALS-g2	12	-2.7 %	-1.9	1.4 %	15	1.8 %
NorESM1-M	8.1	-2.0 %	-1.2	1.4 %	8.6	3.5 %
BNU-ESM	8.2	-2.1 %	-0.80	2.7 %	5.9	3.6 %
CMCC-CESM	8.9	-1.9 %	-0.56	3.1 %	5.2	2.0 %
BCC-CSM1.1	11	-0.97%	-1.8	4.0 %	15	6.3 %
IPSL-CM5B-LR	11	-2.1 %	-3.3	4.4 %	48	5.8 %
MPI-ESM-LR	11	-1.8 %	-1.00	4.6 %	7.4	4.8 %
CNRM-CM5	11	-1.1 %	-1.9	5.4 %	20	8.3 %
GFDL-CM3	8.5	-1.7 %	-1.4	6.2 %	13	10 %
CCSM4	9.0	-1.4 %	-1.8	6.2 %	17	10 %
GFDL-ESM2M	8.9	-1.4 %	-1.6	16 %	18	28 %
IPSL-CM5A-LR	8.8	-1.2 %	-1.1	21 %	14	23 %
GFDL-ESM2G	8.7	-1.1 %	-1.3	22 %	12	49 %
Transient CO ₂ increase						
IPSL-CM5B-LR	12	-2.1%	-3.2	2.3%	46	4.0%
MIROC5	10	-2.0%	-1.4	4.4%	10	6.5%
GFDL-ESM2G	8.8	-1.0%	-1.2	11 %	10	22 %
IPSL-CM5A-MR	9.5	-2.1%	-1.4	14 %	18	19 %
GFDL-ESM2M	8.9	-1.8%	-1.3	19 %	12	38 %
IPSL-CM5A-LR	9.1	-2.7%	-0.86	27 %	11	26 %
Abrupt CO ₂ increase						
MIROC-ESM	9.3	-2.6 %	-0.65	0.29%	5.6	0.75%
IPSL-CM5B-LR	12	-2.3 %	-3.3	3.0 %	48	5.1 %
MIROC5	10	-1.9 %	-1.4	4.2 %	10	5.8 %
CanESM2	9.3	-0.64%	-1.0	5.2 %	9.6	6.2 %
MPI-ESM-LR	11	-1.4 %	-0.91	5.8 %	7.0	4.7 %
MRI-CGCM3	11	0.84 %	-2.0	17 %	20	35 %
IPSL-CM5A-MR	9.5	-1.0 %	-1.4	20 %	18	31 %
IPSL-CM5A-LR	9.1	-1.4 %	-0.87	25 %	11	27 %

772 **LIST OF FIGURES**

773 **Fig. 1.** The CMIP5 multi-model mean distributions of daily (a) rain frequency (with dry-day fre-
774 quency at top left) and (b) rain amount, and the response of (c) rain frequency and (d) rain
775 amount to increasing carbon dioxide, following Pendergrass and Hartmann (2014b). Change
776 in dry-day frequency ($\% \text{ K}^{-1}$) is noted in the top left corner of panel c. Error intervals are
777 the 95% confidence limits according to the student's t -test. 44

778 **Fig. 2.** The rain frequency (left) and amount (right) responses to (a-b, purple) an increase mode
779 of 0.9%, (c-d, turquoise) a shift mode of 3.3%, (e-f, magenta) a shift mode of 3.3% and
780 increase mode of 0.9%, and (g-h, orange) equal magnitude shift and increase of 3.3%. The
781 color scheme corresponds to these modes throughout the paper. The initial distribution is
782 shown in Fig 3. 45

783 **Fig. 3.** The distributions driving the first model, where vertical velocity is prescribed: (a) tempera-
784 ture and moisture, and (b) vertical velocity (skewness is noted in the top right corner). The
785 resulting distributions of (c) rain frequency (dry frequency, when rain rate is equal to zero,
786 is noted in the bottom left corner) and (d) rain amount. 46

787 **Fig. 4.** Experiments with the first model. (left) Prescribed vertical velocity distribution, with the
788 initial distribution in the gray-dashed line and each experiments' distribution black in solid
789 back (skewness noted at top right of each panel). (center) Predicted rain frequency response
790 (change in dry frequency noted at center-left). (right) Predicted rain amount response in
791 black, with the fitted shift-plus-increase response in color. Colors correspond to Fig. 2; the
792 magnitude of the fitted shift and increase modes and their errors are listed in Table 2. Each
793 row is one experiment: (a-c) warm, (d-f) weaken the vertical velocity distribution, (g-i) skew
794 the vertical velocity distribution, (j-l) warm and skew, and (m-o) warm while weakening and
795 skewing the vertical velocity distribution. 47

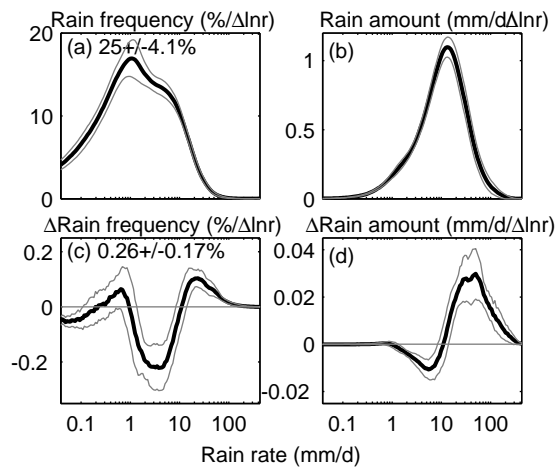
796 **Fig. 5.** The prescribed (top) distributions driving the second model, where vertical velocity is pre-
797 dicted: (a) temperature and moisture, and (b) non-latent heating (mean is noted in the top-
798 right corner). The resulting predicted (bottom) distributions of (c) vertical velocity, (d) rain
799 frequency (dry frequency noted in the bottom left corner) and (e) rain amount. 48

800 **Fig. 6.** Experiments varying parameters other than the mean temperature with the second model,
801 following Fig. 4 but here the vertical velocity distribution (left) is predicted. (a-c) Increasing
802 the magnitude of mean non-latent heating and increasing the width of the non-latent heating
803 distributions, while holding all other parameters constant. (d-f) Increasing the magnitude
804 of mean non-latent heating and decreasing stability. (g-i) Narrowing the non-latent heating
805 distribution (decreasing σ_{Q_n}) and decreasing stability. Note the smaller y axis magnitudes in
806 panels h and i. 49

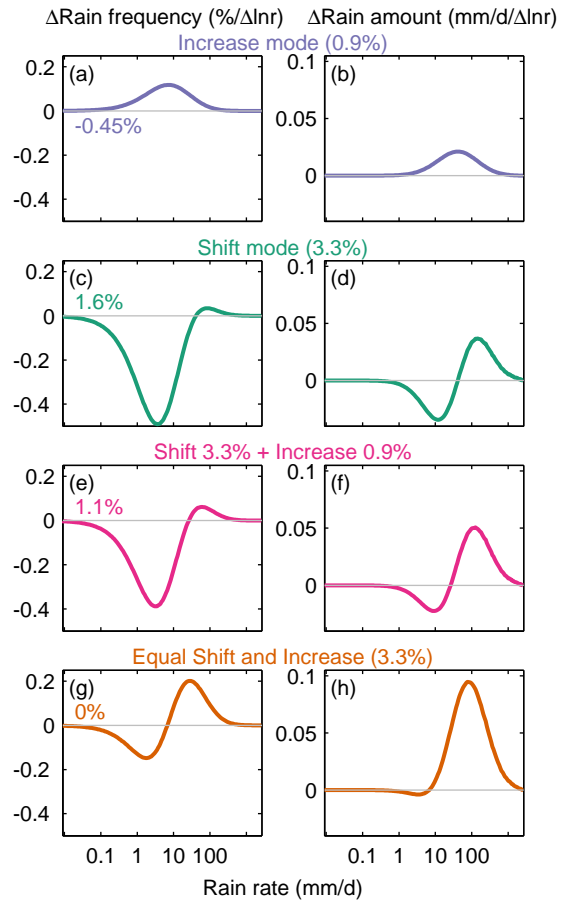
807 **Fig. 7.** Experiments warming while varying one other parameter with the second model, following
808 Fig. 6: (a-c) increasing stability, (d-f) increasing the magnitude of mean non-latent heating,
809 and (g-i) narrowing the non-latent heating distribution (decreasing σ_{Q_n} , note the smaller y
810 axis magnitudes in panels h and i). 50

811 **Fig. 8.** Experiments warming, increasing the magnitude of the non-latent heating distribution by
812 the value from climate models, $1.1 \text{ W m}^{-2} \text{ K}^{-1}$, while varying one other parameter with the
813 second model, following Fig. 6: (a-c) increasing stability, and (d-f) narrowing the non-latent
814 heating distribution (decreasing σ_{Q_n}). 51

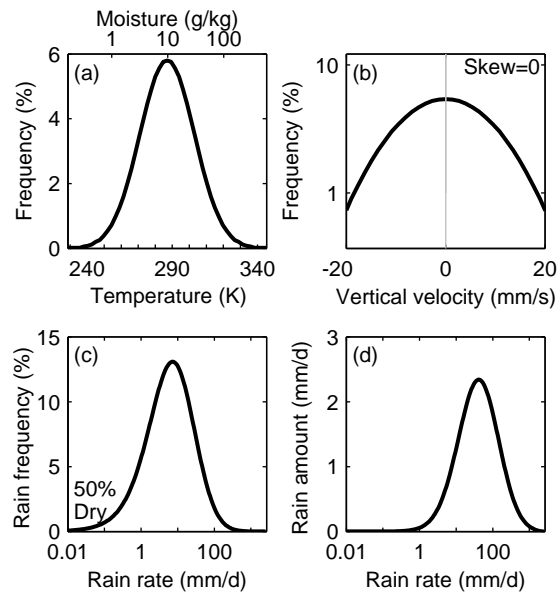
815 **Fig. 9.** A schematic showing the effects of changing width and skewness of the vertical velocity
816 distribution. An initial skewed distribution of w (a), is perturbed by (b) decreasing its stan-
817 dard deviation, (c) increasing its skewness, and (d) both decreasing standard deviation and
818 increasing skewness together. 52



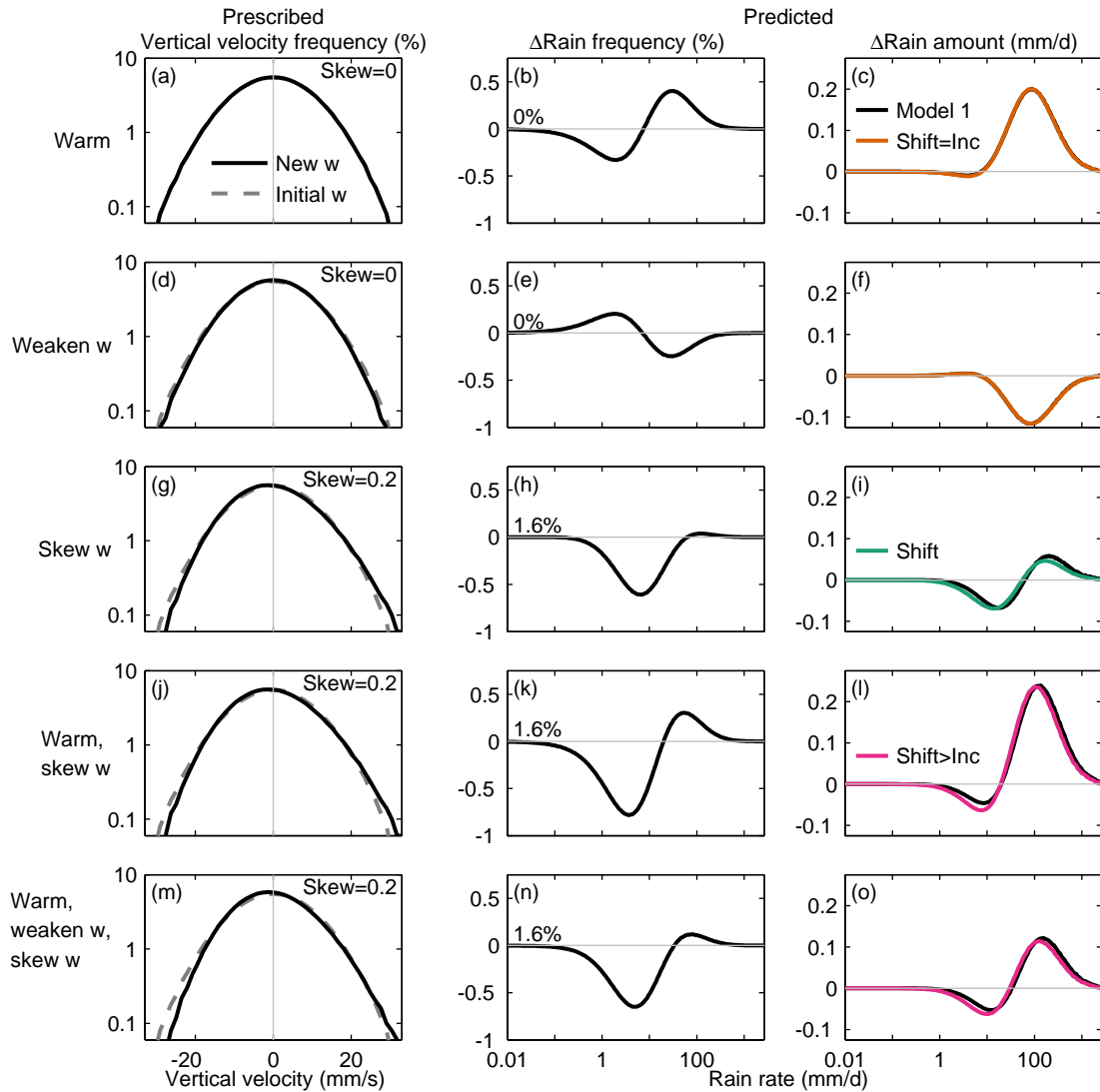
819 FIG. 1. The CMIP5 multi-model mean distributions of daily (a) rain frequency (with dry-day frequency at
 820 top left) and (b) rain amount, and the response of (c) rain frequency and (d) rain amount to increasing carbon
 821 dioxide, following Pendergrass and Hartmann (2014b). Change in dry-day frequency ($\% K^{-1}$) is noted in the
 822 top left corner of panel c. Error intervals are the 95% confidence limits according to the student's t -test.



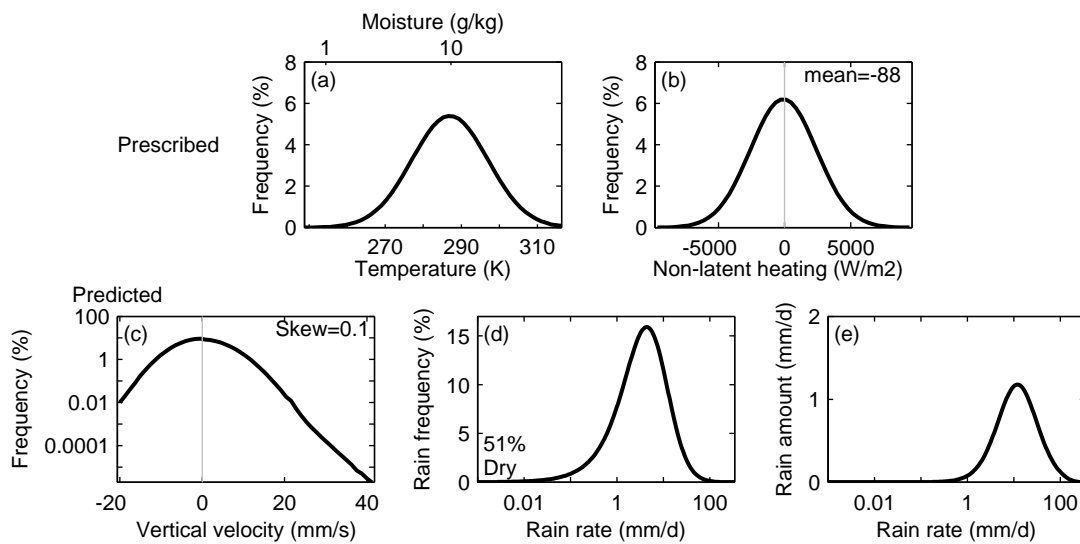
823 FIG. 2. The rain frequency (left) and amount (right) responses to (a-b, purple) an increase mode of 0.9%,
 824 (c-d, turquoise) a shift mode of 3.3%, (e-f, magenta) a shift mode of 3.3% and increase mode of 0.9%, and (g-h,
 825 orange) equal magnitude shift and increase of 3.3%. The color scheme corresponds to these modes throughout
 826 the paper. The initial distribution is shown in Fig 3.



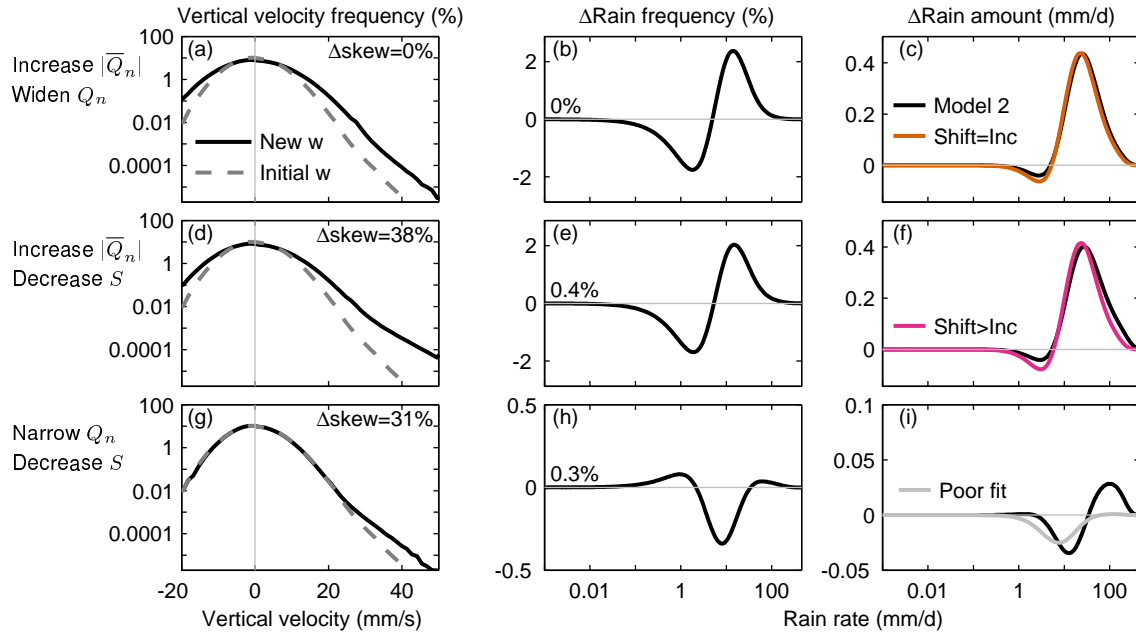
827 FIG. 3. The distributions driving the first model, where vertical velocity is prescribed: (a) temperature and
 828 moisture, and (b) vertical velocity (skewness is noted in the top right corner). The resulting distributions of (c)
 829 rain frequency (dry frequency, when rain rate is equal to zero, is noted in the bottom left corner) and (d) rain
 830 amount.



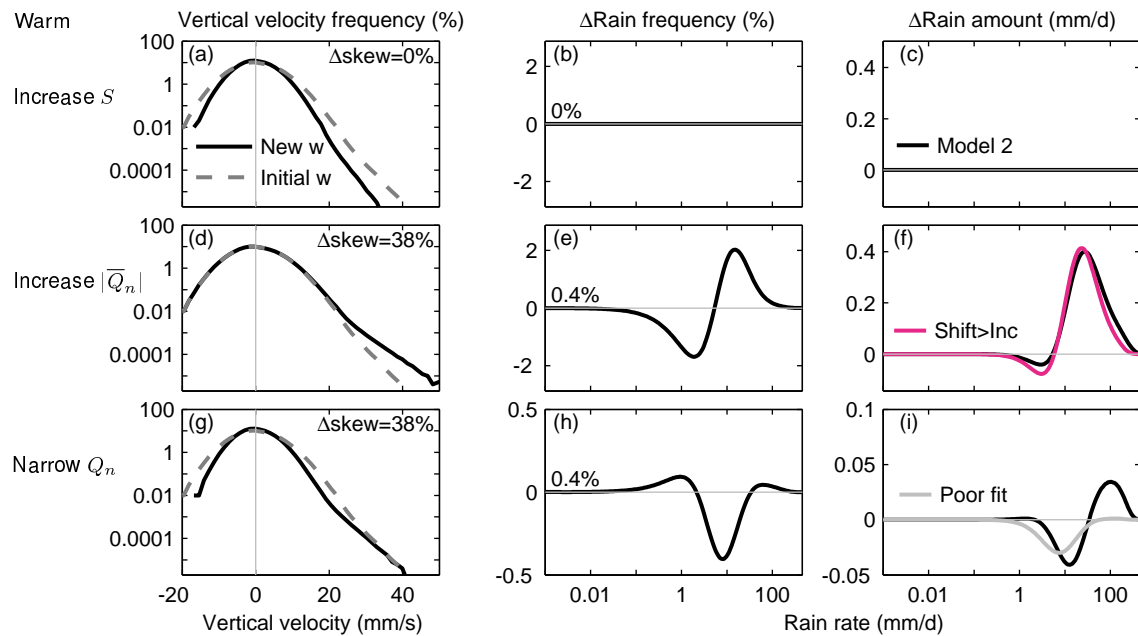
831 FIG. 4. Experiments with the first model. (left) Prescribed vertical velocity distribution, with the initial
 832 distribution in the gray-dashed line and each experiments' distribution black in solid back (skewness noted at
 833 top right of each panel). (center) Predicted rain frequency response (change in dry frequency noted at center-
 834 left). (right) Predicted rain amount response in black, with the fitted shift-plus-increase response in color. Colors
 835 correspond to Fig. 2; the magnitude of the fitted shift and increase modes and their errors are listed in Table 2.
 836 Each row is one experiment: (a-c) warm, (d-f) weaken the vertical velocity distribution, (g-i) skew the vertical
 837 velocity distribution, (j-l) warm and skew, and (m-o) warm while weakening and skewing the vertical velocity
 838 distribution.



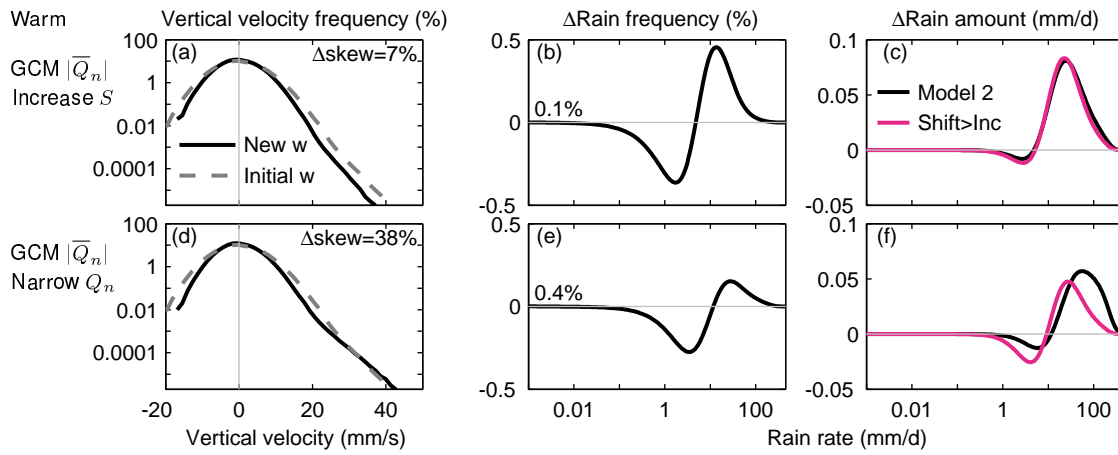
839 FIG. 5. The prescribed (top) distributions driving the second model, where vertical velocity is predicted:
 840 (a) temperature and moisture, and (b) non-latent heating (mean is noted in the top-right corner). The resulting
 841 predicted (bottom) distributions of (c) vertical velocity, (d) rain frequency (dry frequency noted in the bottom
 842 left corner) and (e) rain amount.



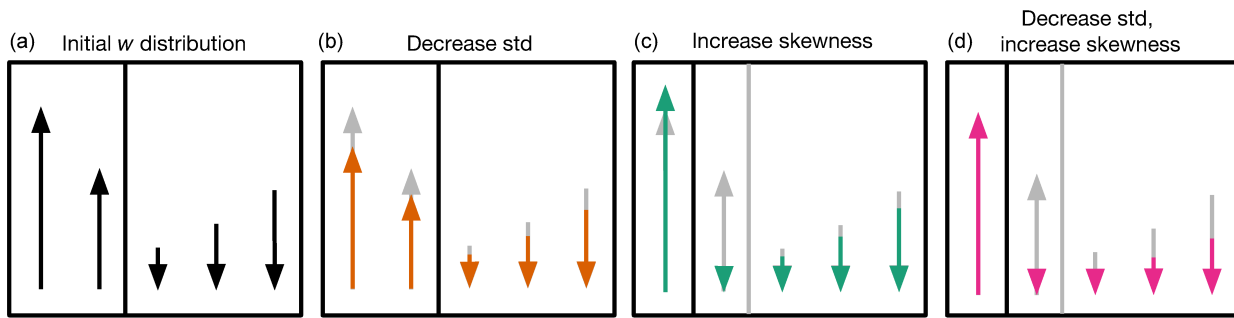
843 FIG. 6. Experiments varying parameters other than the mean temperature with the second model, following
 844 Fig. 4 but here the vertical velocity distribution (left) is predicted. (a-c) Increasing the magnitude of mean non-
 845 latent heating and increasing the width of the non-latent heating distributions, while holding all other parameters
 846 constant. (d-f) Increasing the magnitude of mean non-latent heating and decreasing stability. (g-i) Narrowing
 847 the non-latent heating distribution (decreasing σ_{Q_n}) and decreasing stability. Note the smaller y axis magnitudes
 848 in panels h and i.



849 FIG. 7. Experiments warming while varying one other parameter with the second model, following Fig. 6:
 850 (a-c) increasing stability, (d-f) increasing the magnitude of mean non-latent heating, and (g-i) narrowing the
 851 non-latent heating distribution (decreasing σ_{Q_n} , note the smaller y axis magnitudes in panels h and i).



852 FIG. 8. Experiments warming, increasing the magnitude of the non-latent heating distribution by the value
 853 from climate models, $1.1 \text{ W m}^{-2} \text{ K}^{-1}$, while varying one other parameter with the second model, following
 854 Fig. 6: (a-c) increasing stability, and (d-f) narrowing the non-latent heating distribution (decreasing σ_{Q_n}).



855 FIG. 9. A schematic showing the effects of changing width and skewness of the vertical velocity distribution.
 856 An initial skewed distribution of w (a), is perturbed by (b) decreasing its standard deviation, (c) increasing its
 857 skewness, and (d) both decreasing standard deviation and increasing skewness together.